

1

Nonlinear dynamics of surface steps*Joachim Krug*

1.1

Introduction

Surface steps are key elements in the dynamics of a crystal surface below its thermodynamic roughening transition, because they constitute long-lived structural defects which are nevertheless highly mobile and prone to strong fluctuations [1]. The description of surface morphology evolution in terms of the thermodynamics and kinetics of steps goes back at least half a century [2]. During the past few decades the subject has experienced a significant revival due to the availability of imaging methods such as scanning tunneling microscopy, which allow for a direct visualization of step conformation and step motion on the nanoscale; see [3–7] for recent reviews. In this chapter I will focus specifically on cases where steps have been found to display complex *dynamic* behavior, such as oscillatory shape evolution under constant driving.

The examples to be discussed below can be naturally organized according to the underlying topology of the step configurations: We first consider driven single-layer islands (closed step loops), and then vicinal surfaces (arrays of parallel steps). A certain familiarity with the basic thermodynamics and kinetics of crystal surfaces is assumed; for an elementary introduction the reader may consult [8].

1.2

Electromigration-driven islands and voids

Electromigration is the directed transport of matter in a current-carrying material, which is caused (primarily) by the scattering of conduction electrons off defects such as interstitials or atoms adsorbed on the surface (henceforth referred to as *adatoms*), see Fig.1.1 for a sketch. Much of the work on electromigration has been motivated by its importance as a damage mechanism limiting the lifetime of integrated circuits [9]. Because electromigration forces are small compared to the typical energy barriers involved in the thermal dif-

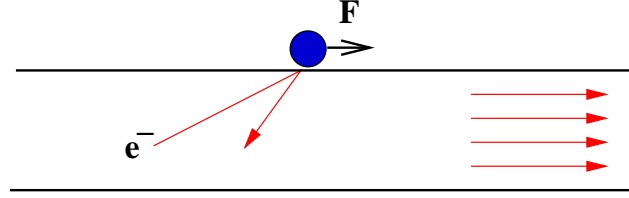


Fig. 1.1 Schematic of the microscopic origin of the electromigration force: Conduction electrons scattering off an adatom give rise to a transfer of momentum in the direction of the current flow.

fusion of atoms, the direct observation of electromigration effects in real time on atomistic length scales is difficult (see, however, [10] for recent progress in this direction). In this chapter the electromigration force will be used as a conceptually simple way of driving a system of surface steps out of equilibrium, giving rise to surprisingly complex dynamical behavior.

1.2.1

Electromigration of single layer islands

Two-dimensional single-layer islands are the simplest nanoscale structures that appear on a surface during the early stages of thin film growth, when the amount of deposited material is a small fraction of a monolayer [5]. Because of their small size, such islands display considerable shape fluctuations already in thermal equilibrium, which may cause diffusive motion of the island as a whole [4]. The electromigration-induced drift of single-layer islands on the Si(111) surface was observed experimentally by Métois and collaborators in 1999 [11]. In the following we summarize recent theoretical work on this problem, which is based on a continuum formulation due to Pierre-Louis and Einstein [12].

We focus here on the simplest case where the motion of atoms is restricted to the boundary of the islands, such that the island area is conserved¹. Then the local normal velocity v_n of the island boundary satisfies a continuity equation,

$$v_n = -\frac{\partial}{\partial s} j = \frac{\partial}{\partial s} \sigma \left[\frac{\partial}{\partial s} (\tilde{\gamma} \kappa) - F_t \right], \quad (1.1)$$

where s denotes the arclength measured along the island contour. The mass current j along the island boundary is proportional to the step edge mobility σ , and it is driven by capillary forces and the tangential (to the boundary) component F_t of the electromigration force. The capillary force, in turn, is given by the tangential gradient of the edge chemical potential, which is the product of the edge stiffness $\tilde{\gamma}$ and the edge curvature κ . The stiffness $\tilde{\gamma}$ is derived

¹) A nonconserved situation where the step exchanges atoms with the terrace is treated below in Sect.1.2.4.

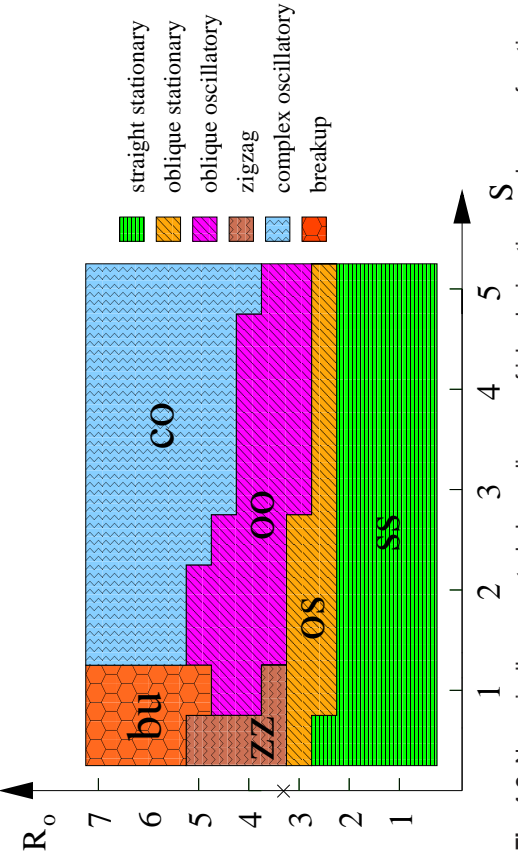


Fig. 1.2 Numerically generated phase diagram of island migration modes as a function of the anisotropy strength S_0 , as defined in (1.5), and the dimensionless island radius $R_0 = R/l_E$. In the regions denoted by **zz** and **oo** the island shape oscillates periodically, while in the **co** region the behavior is irregular, possibly chaotic. The cross on the R_0 -axis indicates the bifurcation from circular to elongated shapes in the isotropic case at the critical radius (1.3). The phase diagram is based on a grid of resolution 0.5×0.5 in the S - R_0 -plane.

from the edge free energy per unit length γ according to $\tilde{\gamma} = \gamma + \gamma''$, where primes denote derivatives with respect to the orientation angle of the edge. In the absence of external forces ($F_t = 0$) Eq.(1.1) guarantees the relaxation of the island to its equilibrium shape characterized by $\tilde{\gamma}\kappa = \text{const.}$ [5]. Throughout this section the electromigration force is assumed to be constant in magnitude and direction. This implies that

$$F_t = F_0 \cos \theta, \quad (1.2)$$

where θ denotes the angle between the boundary and the direction of the force.

In the absence of crystalline anisotropy the material parameters σ and $\tilde{\gamma}$ in (1.1) are constants, and it is straightforward to check that Eqs.(1.1,1.2) are solved by a circle of arbitrary radius R moving at constant speed $V = \sigma F_0/R$ [13]. Linear stability analysis of the circular solution shows that it becomes unstable at a critical radius [14]

$$R_c \approx 3.26 l_E, \quad (1.3)$$

where the characteristic length scale obtained by non-dimensionalizing (1.1) reads

$$l_E = \sqrt{\tilde{\gamma}/F_0}. \quad (1.4)$$

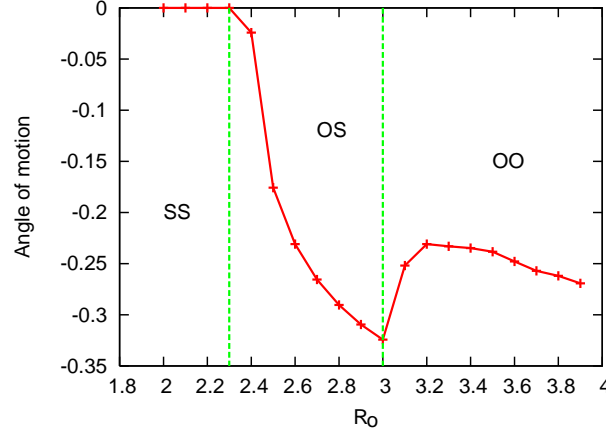


Fig. 1.3 Angle enclosed by the direction of island motion and the direction of the applied force as a function of the scaled island radius for $S = 2$. The transitions between the different phases in Fig.1.2 are manifest as slope discontinuities in this graph.

Beyond the linear instability of the circular solution one finds a family of stationary shapes which are elongated in the direction of the force and become increasingly sensitive to breakup with increasing size [15, 16].

The effect of crystalline anisotropy in the mobility σ was explored, mostly numerically, in [15, 17]. Using the expression [18]

$$\sigma(\theta) = \sigma_0[1 + S \cos^2(n\theta)], \quad (1.5)$$

where $2n$ denotes the number of symmetry axes, a surprisingly rich phase diagram of migration modes was obtained in the plane spanned by the anisotropy strength S and the dimensionless island radius $R_0 = R/l_E$ for the case of sixfold anisotropy ($n = 3$), see Fig.1.2. In these calculations the force was oriented along a direction of maximal mobility.

For small R_0 the dynamics is dominated by capillarity and the island shape is close to the equilibrium shape. The island moves at constant speed in the direction of the applied force (**ss** = straight stationary motion). With increasing size a bifurcation to a regime of oblique stationary (**os**) motion occurs, in which the symmetry with respect to the force direction is spontaneously broken. A suitable order parameter for this bifurcation is the angle between the direction of force and the direction of motion (Fig.1.3). Increasing the radius further another bifurcation occurs to a phase in which the obliquely moving island displays periodic shape oscillations (the **oo** phase). At smaller values of S the island performs an oscillatory zig-zag motion which is directed along the applied force on average (Fig.1.4).

A clear signature of the transition from stationary oblique to oscillatory behavior shows up in the angle of island migration (Fig.1.3). In addition, we

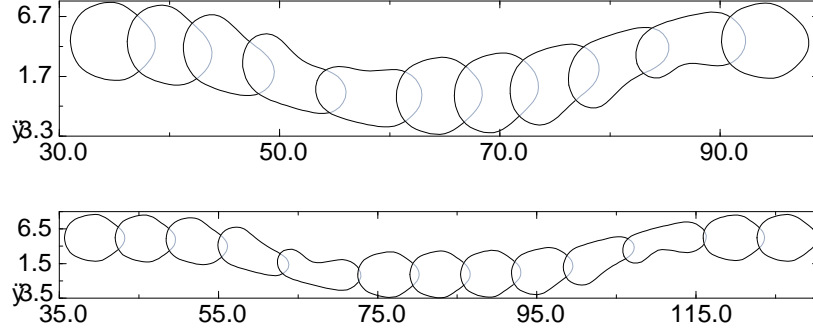


Fig. 1.4 Oscillatory island motion in the zig-zag phase of the phase diagram. Parameters are $R_0 = 3.5, S = 0.5$ for the upper panel and $R_0 = 3.5, S = 1$ for the lower panel. All lengths are measured in units of l_E .

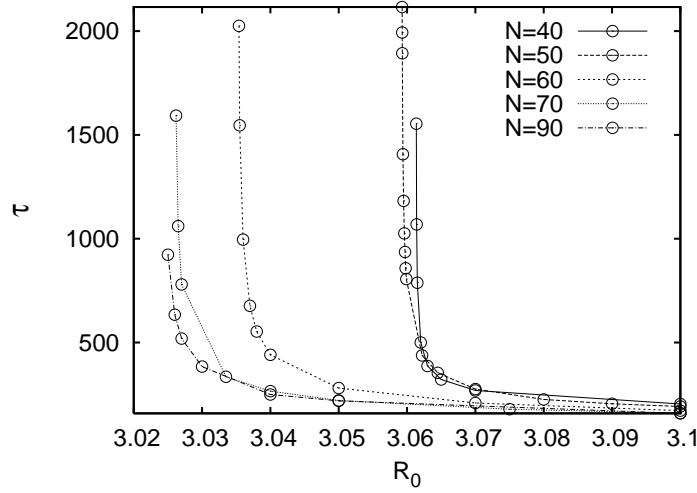


Fig. 1.5 Period τ of the shape oscillation near the transition from the $\infty\infty$ to the ∞s phase. Different curves show results obtained for different numbers N of discretization points in the numerical solution, with N increasing from right to left (from [16]).

observe that the period τ of the shape oscillation diverges as the critical radius $R_0^{\infty\infty}$ of the transition is approached from above (Fig.1.5). Although the data show some dependence on the number of discretization points, a power law fit indicates that the period diverges as

$$\tau \sim (R_0 - R_0^{\infty\infty})^{-2.5}. \quad (1.6)$$

Increasing the island size further the oscillations become increasingly irregular. This is illustrated in Fig.1.6 by the time series of the island perimeter. The uppermost curve in the figure displays large scale fluctuations which can be traced back to reversals of the direction of island motion which occur at

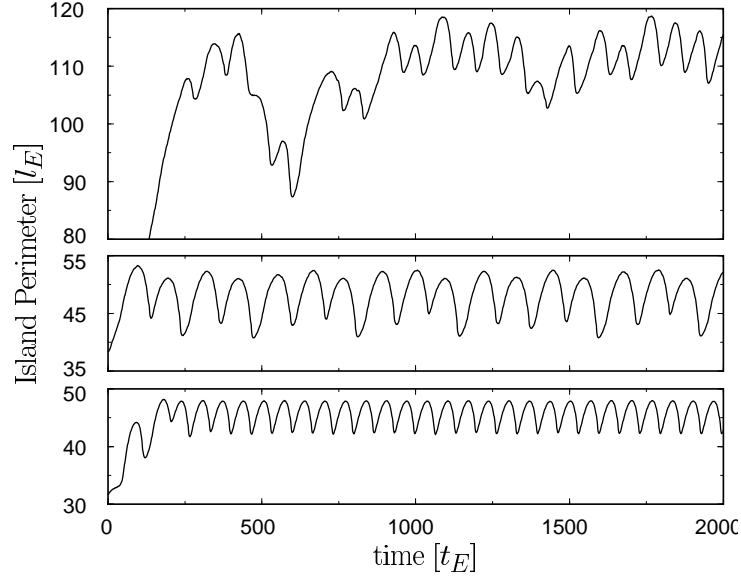


Fig. 1.6 Time series of the island perimeter, measured in units of l_E . From bottom to top, parameters are $S = 2, R_0 = 5$; $S = 5, R_0 = 5$; and $S = 5, R_0 = 6.5$. Time is measured in units of $t_E = l_E^4 / (\sigma_0 \tilde{\gamma})$.

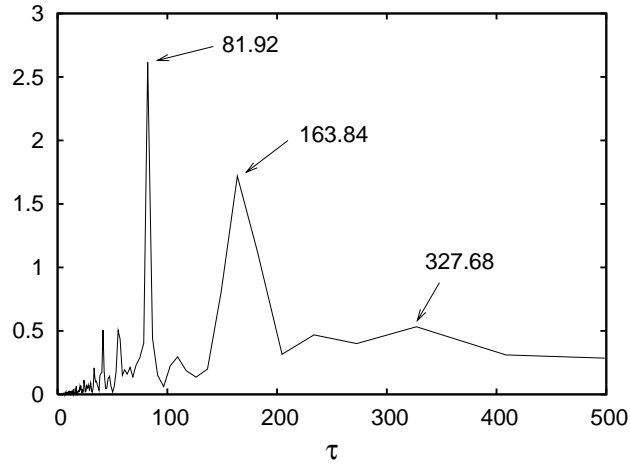


Fig. 1.7 Fourier spectrum of the island perimeter time series for $S = 3$ and $R_0 = 6$, plotted as a function of the period $\tau = 2\pi/\omega$ (from [16]).

irregular intervals [17]. The Fourier spectrum of such a time series is broad and shows clear signatures of period doubling (Fig.1.7).

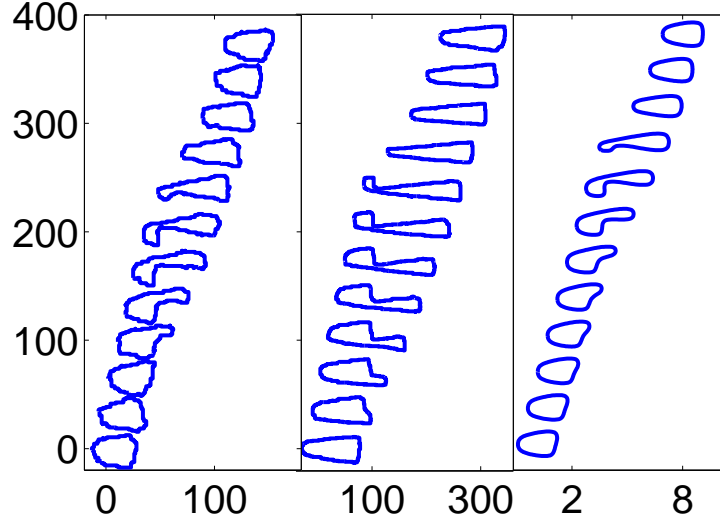


Fig. 1.8 Comparison of island shape evolution obtained from KMC simulations (left and middle columns) and numerical solution of the continuum model (right column). The simulated islands consist of 1000 atoms in the right column and 4000 atoms in the middle column. The left and right columns correspond to a temperature of $T = 700$ K, while in the middle column $T = 500$ K. In the left and middle columns lengths are measured in units of the lattice constant, in the right column in units of l_E .

1.2.2

Continuum vs. discrete modeling

We have seen in the preceding section that electromigration-driven islands display a number of features which are consistent with the behavior of a low-dimensional, non-linear dynamical system. This is remarkable, since physically such an island consists of a large number of atoms which move stochastically under the influence of thermal fluctuations and a very small systematic force.

In order to determine whether the phenomena predicted on the basis of the deterministic continuum model (1.1) persist also under experimentally realistic conditions, extensive Kinetic Monte Carlo (KMC) simulations were carried out using a lattice model that has been shown to provide an accurate representation of metal surfaces² such as Cu(100) [19]. In a suitably chosen range of parameters, a regime of oscillatory motion could be identified which shows dynamic behavior in good, essentially quantitative agreement with the continuum model (Fig.1.8).

² See [5, 7] for an overview of similar models, and [12, 20] for earlier KMC-simulations of island electromigration.

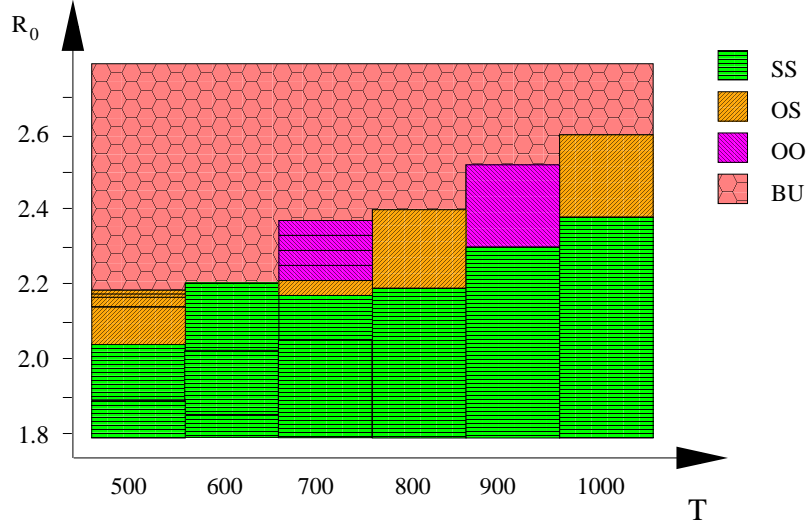


Fig. 1.9 Phase diagram of island migration modes obtained by numerical solution of the continuum equations for a mobility and stiffness of fourfold crystalline anisotropy. The temperature is measured in Kelvin, and the anisotropy increases with decreasing temperature. Temperature was varied in steps of 100 K. Each rectangle corresponds to a single value of R_0 and T , which is located in the center of the rectangle. The cases $T = 500\text{K}$ and $T = 700\text{K}$, which correspond to the KMC simulations, were explored with higher resolution. The abbreviations used for the different phases are explained in Fig.1.2 (from [16]).

For the comparison to KMC simulations, realistic expressions for the step edge mobility σ and the stiffness $\tilde{\gamma}$ in (1.1) were derived and implemented. Both of these quantities display a fourfold anisotropy on the fcc(100) surface. A rough exploration of the full phase diagram, conducted within the continuum model, is depicted in Fig.1.9. Since the physical parameter controlling the anisotropy is the temperature T , with lower temperatures corresponding to more pronounced anisotropy, the temperature axis in Fig.1.9 replaces the anisotropy axis in Fig.1.2. The regions displaying oscillatory behavior without leading to island breakup are much more limited than in the case of six-fold anisotropy. In particular, at $T = 500\text{ K}$ no oscillatory regime was found in the continuum model, despite the fact that oscillations are seen in the KMC simulations at this temperature (middle column in Fig.1.8). This is one of the indications of a breakdown of the continuum description at low temperatures which were reported in [19].

1.2.3

Nonlocal shape evolution: Two-dimensional voids

Formally, the island electromigration problem described in the preceding sections is largely equivalent to the problem of electromigration of cylindrical

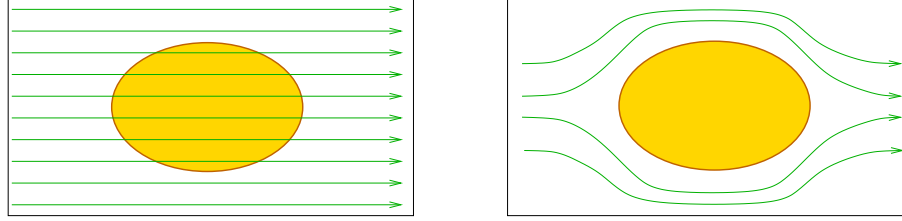


Fig. 1.10 Comparison between the electromigration problem for islands (left) and voids (right). Arrows indicate the flow of the electric current. The shape evolution problem on the left is *local*, whereas on the right one has to solve a *nonlocal* moving boundary value problem.

voids in a thin metallic film. The formation, migration and shape evolution of such voids plays an important part in the failure of metallic interconnects in integrated electronic circuits [9]. In this context the size scale of interest is usually in the range of micrometers, rather than nanometers, but on the level of the continuum description on which (1.1) is based this difference is immaterial.

A more relevant distinction is illustrated in Fig.1.10: In the case of an island on top of a thick metallic substrate, the disturbance of the electric current distribution in the bulk due to the presence of the island can be neglected, and correspondingly the force F_t in (1.1) can be approximated by the simple constant expression (1.2). On the other hand, in the presence of an insulating void in a current-carrying film, the current is obviously forced to flow around the void. As a consequence, the current distribution, and hence the distribution of electromigration forces, is strongly dependent on the void shape itself, and the shape evolution becomes a non-local moving boundary value problem for the electric potential [18]. It is possible to interpolate between the two cases depicted in Fig.1.10 by considering a conducting void and varying the conductivity ratio between the interior and the exterior regions [14].

Oscillatory shape evolution of two-dimensional voids was first observed numerically by Gungor and Maroudas [21]. They considered edge voids located at the boundary of a two-dimensional conducting strip. In the presence of crystalline anisotropy in the mobility of adatoms along the inner void surface, a transition from stationary to oscillatory behavior occurs with increasing electromigration force or void area. Subsequent detailed analysis has shown that this transition has the character of a Hopf bifurcation [22]. The experimental signature of oscillatory void evolution are rapid oscillations in the resistance of the conductor, which have indeed been reported in the literature [23].

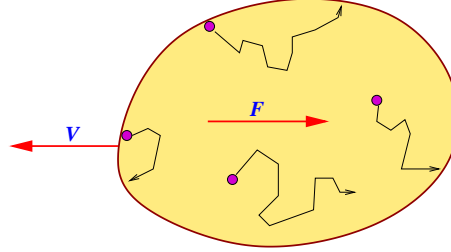


Fig. 1.11 Sketch of a vacancy island migrating by internal terrace diffusion. The drift force leads to a net transport of material from the left to the right, which implies island migration in the opposite direction.

1.2.4

Nonlocal shape evolution: Vacancy islands with terrace diffusion

The exchange of atoms between the step and the surrounding terraces is another source of nonlocality in the motion of the steps, since it necessitates the solution of a moving boundary value problem for the concentration of adatoms on the terraces [2,8]. A particular case in this class of problems is the *interior model* for the electromigration of vacancy islands introduced in [12], and studied in detail in [16,24].

As illustrated in Fig.1.11, one considers a vacancy island (i.e. a surface region which is one atomic height lower than the surrounding terrace) bounded by an ascending step. Atoms can detach from the step and diffuse across the island, but an energy barrier prevents atoms from entering the island from the exterior terrace. This leads to a moving boundary value problem in the bounded interior domain, where the adatom concentration $\rho(\vec{r}, t)$ satisfies the drift-diffusion equation

$$\frac{\partial \rho}{\partial t} = D \nabla^2 \rho - \frac{D}{k_B T} \vec{F} \cdot \nabla \rho \quad (1.7)$$

with appropriate boundary conditions at the step edge (see [8] for a general discussion). If the exchange of atoms with the step edge is rapid, so that thermal equilibrium is maintained at the boundary at all times, a circular stationary solution drifting at constant speed against the force direction can be found [12].

From the perspective of nonlinear dynamics, an intriguing feature of this problem is that the circular solution is linearly stable, although numerical simulation of the fully nonlinear evolution shows that the circle develops an instability (leading eventually to the pinching off of a small island) under finite perturbations [24]. The critical perturbation strength needed to trigger the

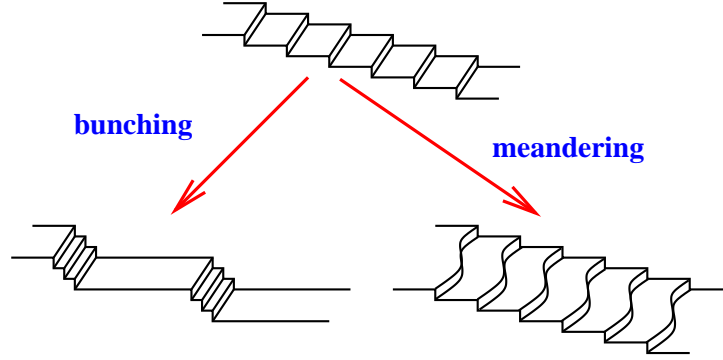


Fig. 1.12 Schematic of the two main morphological instabilities of a vicinal surface.

instability decreases as the dimensionless island size, defined in this case by

$$R_0 = \frac{R}{\xi}, \quad \xi = \frac{k_B T}{|\vec{F}|}, \quad (1.8)$$

is increased by increasing either the force or the island size. A similar scenario combining linear stability with nonlinear instability was previously found in the problem of two-dimensional void migration [18,25] as well as in the dynamics of ionization fronts [26,27].

The effects of crystalline anisotropy in this problem have not been explored so far. However, in view of the results described in the preceding subsections, it seems likely that oscillatory and other modes of complex shape evolution may arise in this case as well.

1.3

Step bunching on vicinal surfaces

A vicinal surface is obtained by cutting a crystal at a small angle relative to a high symmetry orientation, such that a staircase of well-separated, atomic height steps forms. When such an array of steps is set into motion by growing or sublimating the crystal, or by applying an electromigration force on the adatoms, a variety of patterns emerges.

Quite generally, the pattern formation process can be understood as a competition between the destabilizing effects of the external forces, and thermodynamic forces arising from the step free energy and repulsive step-step interactions, which act to restore the equilibrium state of straight, equidistant steps. The resulting instability scenarios have been studied extensively on the level of linear stability analysis, see e.g. [28]. The two basic modes of instability are illustrated in Fig.1.12: In *step bunching* the individual steps remain straight but

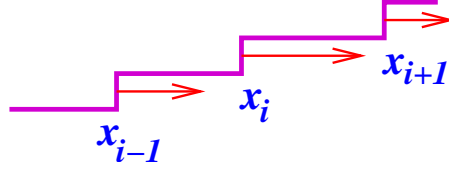


Fig. 1.13 Sketch of a one-dimensional step train. Under sublimation, ascending steps move to the right.

the initially homogeneous step train breaks up into regions of high step density (bunches) separated by wide terraces. By contrast, in *step meandering* the individual steps become wavy; often the repulsive interactions between the steps then force the different steps to meander in phase, such that an overall periodic surface corrugation perpendicular to the direction of vicinality results. In some cases step bunching and step meandering have been observed to coexist [29, 30].

In the following some recent results on the *nonlinear* evolution of step bunches will be summarized, focusing again on instances of complex *temporal* behavior of the step configurations. For a discussion of the nonlinear dynamics of meandering steps we refer to [31].

When step bunching is the dominant instability, the steps can (to a first approximation) be assumed to be straight, and the problem reduces to the one-dimensional motion and interaction of point-like steps. Figure 1.13 illustrates the situation for the case of *sublimation*, where ascending steps move (on average) to the right. The equations of motion for the steps can be obtained from the solution of a one-dimensional moving boundary value problem for the adatom concentration on the terraces. This procedure has been reviewed in detail elsewhere [8]. Here we start the discussion directly from the nonlinear equations of motion, regarded as a (physically motivated) many-dimensional dynamical system.

1.3.1

Stability of step trains

As a first orientation, suppose the velocity \dot{x}_i of the i 'th step is the sum of contributions f_+ and f_- , which are functions of the length of the leading terrace (in front of the step) and the trailing terrace (behind the step), respectively, such that

$$\frac{dx_i}{dt} = f_+(x_{i+1} - x_i) + f_-(x_i - x_{i-1}) \quad (1.9)$$

for the N steps $i = 1, \dots, N$, and periodic boundary conditions are employed. Then a uniform step train of equally spaced steps,

$$x_i^{(0)} = il + vt \quad (1.10)$$

is always a solution, with l denoting the step spacing and $v = f_+(l) + f_-(l)$ the step speed. A straightforward linear stability analysis of (1.9) reveals that the solution (1.10) is stable if

$$\frac{d}{dx}[f_+(x) - f_-(x)]|_{x=l} > 0, \quad (1.11)$$

and step bunching occurs when this condition is violated.

There are obviously different ways in which such an instability can be realized. One possibility is that both contributions on the right hand side of (1.9) are increasing functions of the terrace size, but the contribution from the trailing terrace is larger, i.e. the step motion is primarily driven from behind. This is the scenario first described by Schwoebel and Shipsey [32, 33], who pointed out that the preferential attachment/detachment of adatoms from/to the lower terrace bordering a step leads to step bunching during sublimation. The mechanism for electromigration-induced step bunching first described by Stoyanov [34] is of a similar nature. We will return to this case in the following sections.

A different scenario was investigated by Kandel and Weeks [35, 36], who considered a class of one-sided models with $f_- \equiv 0$ and a *nonmonotonic* function f_+ of the form

$$f_+(x) = cx(x_0 - x). \quad (1.12)$$

This work was motivated by the physics of impurity-induced step bunching during growth, where steps are slowed down by impurities that accumulate on the terraces [37, 38]. Larger terraces have been exposed to the impurity flux for longer times, which leads to a decrease of the step speed and ultimately to its vanishing when $x = x_0$. The equidistant step train is stable for $l < x_0/2$ and unstable for $l > x_0/2$. Perturbing a single step in an unstable equidistant step train leads to a disturbance wave which (because of the one-sided nature of the dynamics) travels backwards, leaving behind a frozen configuration of step bunches separated by terraces of size x_0 . Varying the initial step spacing one finds a sequence of spatial bunching patterns, which can be periodic, intermittent or chaotic³.

³ A similar scenario has been found in a model for sand ripple formation in an oscillatory flow [39].

1.3.2

Strongly and weakly conserved step dynamics

An important global characteristic of the step dynamics is the overall sublimation (or growth) rate of the crystal, which is given by

$$\mathcal{R} = \frac{1}{N} \sum_i \frac{dx_i}{dt}. \quad (1.13)$$

We distinguish between *strongly conserved* step dynamics in which $\mathcal{R} = 0$, and *weakly conserved* dynamics where \mathcal{R} is nonzero but independent of the step configuration⁴. The latter case is realized during growth at relatively low temperature, where desorption of adatoms can be neglected and therefore the growth rate is completely determined by the external deposition flux [41].

A generic model that incorporates the strongly and weakly conserved situation is given by

$$\frac{dx_i}{dt} = \gamma_+ \cdot (x_{i+1} - x_i) + \gamma_- \cdot (x_i - x_{i-1}) + U \cdot (2f_i - f_{i+1} - f_{i-1}) \quad (1.14)$$

with

$$f_i = \frac{l^3}{(x_i - x_{i-1})^3} - \frac{l^3}{(x_{i+1} - x_i)^3}. \quad (1.15)$$

These equations were first written down by Liu and Weeks [42] as a model for electromigration-induced step bunching in the presence of sublimation⁵. In contrast to (1.9), here γ_{\pm} and U are constant coefficients multiplying the terms in parenthesis. Comparison with (1.9) shows that f_{\pm} are linear functions with slopes γ_{\pm} , such that the stability condition reads $\gamma_+ > \gamma_-$. In addition to the linear terms depending on the nearest neighbor step positions, (1.14) contains nonlinear next-nearest-neighbor contributions arising from repulsive thermodynamic step-step interactions of entropic and elastic origin [3,8], which drive the relaxation of the step train to its (equidistant) equilibrium shape.

The sublimation rate for the model (1.14) is $\mathcal{R} = (\gamma_+ + \gamma_-)l$, hence for strongly conserved dynamics one has to set $\gamma_+ = -\gamma_-$. This case is realized in electromigration-induced step bunching without growth or sublimation [43]. In the following we will focus on the weakly conserved case, where $\mathcal{R} > 0$. It is then convenient to normalize the time scale such that $\gamma_+ + \gamma_- = 1$, and to introduce the asymmetry parameter b through [44]

$$\gamma_+ = \frac{1-b}{2}, \quad \gamma_- = \frac{1+b}{2}, \quad (1.16)$$

⁴ In [40] only the *strongly* conserved case is referred to as “conserved”. The reason for our choice of nomenclature will become clear below in Sect.1.3.6.

⁵ We will see below in Sect.1.3.6 that the weakly conserved form (1.14) is in fact not really appropriate in the presence of sublimation.

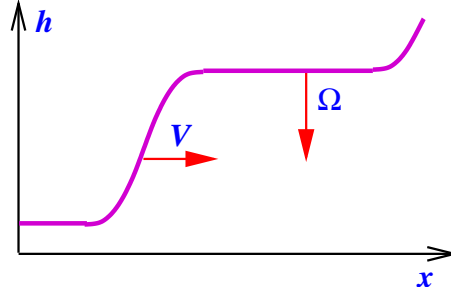


Fig. 1.14 Sketch of a moving step bunch.

such that step bunching occurs for $b > 0$. Together Eqs.(1.14,1.15,1.16) define a two-parameter family of nonlinear many-body problems which have been investigated in detail in [44–46]. In the following two sections some pertinent results of this study will be summarized.

1.3.3

Continuum limit, traveling waves and scaling laws

The analysis of the nonlinear dynamics of step bunches is greatly simplified if it is possible to perform a continuum limit of the problem, thus passing from the discrete dynamical system (1.14) to a partial differential equation [8, 47]. Coarse graining the discrete equations of motion (1.14), one arrives first at a “Lagrangian” continuum description for the step positions x_i or the terrace sizes $l_i = x_{i+1} - x_i$ by converting the layer index i into a continuous surface height $h = ih_0$ (here h_0 denotes the height of an elementary step) [43, 48]. In a second step this is transformed into an “Eulerian” evolution equation for the surface height profile $h(x, t)$ or, equivalently, the step density $m = \partial h / \partial x$, which reads, for the model (1.14) [44, 45]

$$\frac{\partial h}{\partial t} + \frac{\partial}{\partial x} \left[-\frac{b}{2m} - \frac{1}{6m^3} \frac{\partial m}{\partial x} + \frac{3U}{2m} \frac{\partial^2 (m^2)}{\partial x^2} \right] + 1 = 0. \quad (1.17)$$

To unburden the notation, we have normalized vertical and horizontal lengths by setting $h_0 = l = 1$. In the weakly conserved case the evolution law has the form of a continuity equation, with the corresponding current given by the terms inside the square brackets.

The solution $h(x, t) = x/l - t$ of (1.17) is linearly unstable for $b > 0$. The physically relevant nonlinear solutions take the form of a generalized traveling wave,

$$h(x, t) = f(x - Vt) - \Omega t \quad (1.18)$$

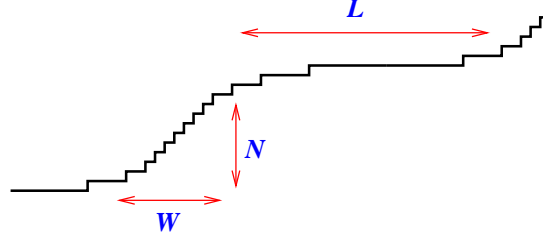


Fig. 1.15 Quantities characterizing the shape of a step bunch.

as illustrated in Fig.1.14. The conserved nature of (1.17) implies the sum rule

$$\Omega + V = 1, \quad (1.19)$$

but the individual values of the vertical and horizontal speed are not fixed by the ansatz⁶. An analysis of periodic solutions of the discrete equations of motion shows that, under rather general conditions,

$$V \sim 1/N. \quad (1.20)$$

Since the mean velocity of a single step is unity in the present units, this implies that bunches move more slowly than steps. Similar to cars in a traffic jam, steps join the bunch from behind, move slowly through the bunch, and accelerate into the *outflow region* which separates one bunch from the next⁷.

Inserting (1.18) into (1.17) one arrives at a third order nonlinear ODE, which can, to a large extent, be handled analytically [44]. A key result are scaling laws [50] for the shape of stationary bunches. As illustrated in Fig.1.15, the shape can be characterized by the bunch width W and the bunch spacing L , both of which are functions of the number N of steps in the bunch. The global constraint on the average slope of the surface implies that $L \sim N$, but the bunch width typically scales with a sublinear power of N , which implies that bunches become steeper as more steps are added. Related quantities of interest are the minimal terrace size l_{\min} in the bunch and the size l_1 of the first terrace in the bunch. On the basis of the continuum equation (1.17) one finds that, asymptotically for large N [44]

$$W \approx 4.1(UN/b)^{1/3}, \quad l_{\min} \approx 2.4(U/bN^2)^{1/3}, \quad l_1 \approx (2U/bN)^{1/3}, \quad (1.21)$$

in good agreement with numerical simulations of the discrete model [45]. Note that $W \sim Nl_{\min}$, as one would expect, but $l_1 \gg l_{\min}$. An experimental study of the shapes of electromigration-induced step bunches on Si(111) is consistent with $l_{\min} \sim N^{-2/3}$ [51].

- 6) For the relation of this problem to the standard velocity selection problem for traveling waves moving into unstable states see [49].
 7) Note however that traffic jams generally move in the direction *opposite* to the traffic flow [52,53].

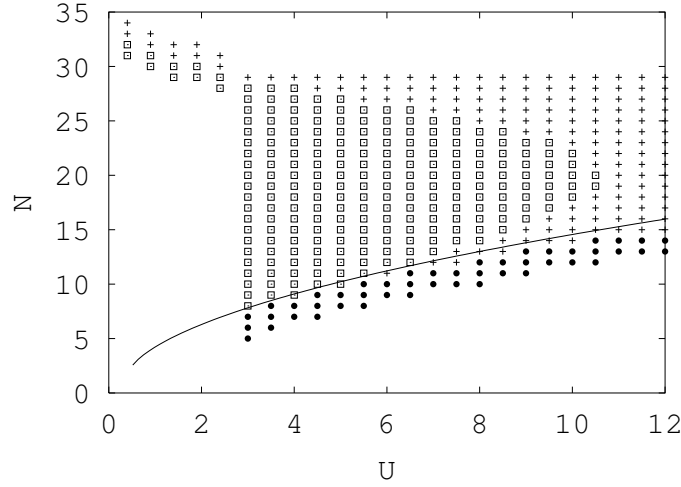


Fig. 1.16 Phase diagram for the behavior of step bunches at $b = 11$. The line is the linear stability limit, below which the equidistant step train is stable (full circles). In the linearly unstable regime above this line bunches either eject no steps (open squares) or they eject one step at a time (crosses).

1.3.4

A dynamic phase transition

As with any hydrodynamic description, the validity of the continuum limit passing from (1.14) to (1.17) is restricted to step configurations in which the step density is slowly varying on the scale of the mean step spacing. To check the consistency of this assumption, we consider the outflow region of the bunch, where the spacing between steps leaving the bunch becomes large and hence the nonlinear interaction terms on the right hand side of (1.14) can be neglected. We are thus left with the linear system

$$\frac{dx_i}{dt} = \frac{1-b}{2}(x_{i+1} - x_i) + \frac{1+b}{2}(x_i - x_{i-1}), \quad (1.22)$$

which can be solved by the exponential traveling wave ansatz

$$l_i \equiv x_{i+1} - x_i = Ae^{Q(i+\Omega t)}. \quad (1.23)$$

Inserting (1.23) into (1.22) yields the relation

$$b = \frac{\sinh Q - \Omega Q}{\cosh Q - 1} \approx \frac{\sinh Q - Q}{\cosh Q - 1}. \quad (1.24)$$

where we have used that $\Omega \rightarrow 1$ for large bunches according to (1.19) and (1.20).

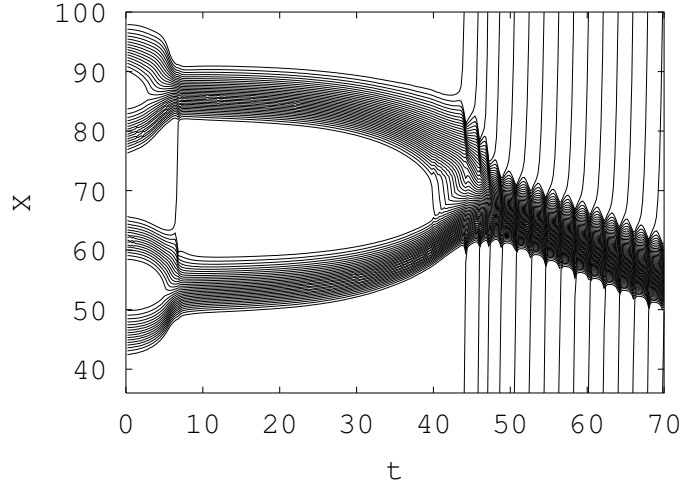


Fig. 1.17 Trajectories of 64 step evolving under the weakly conserved dynamics (1.14) with $b = 20$ and $U = 12$. Step positions are shown in a frame moving with the mean step velocity. Initially the trajectories are horizontal, because the entire bunch moves at the mean step speed.

The step spacing is slowly varying when $Q \ll 1$, which according to (1.24) requires $b \ll 1$. More strikingly, Eq.(1.24) has no solution when $b > 1$. At $b = 1$ the bunch undergoes a *dynamic phase transition* which is reflected, among other things, in the number of “crossing” steps between bunches: For $b < 1$ this number grows with N as $\ln N$, whereas for $b > 1$ at most a single step can reside between two bunches at one time [46].

The physical origin of this change of behavior can be traced back to the evolution equations (1.22). For a step about to leave the bunch the leading terrace is much larger than the trailing terrace, $x_{i+1} - x_i \gg x_i - x_{i-1}$, such that the right hand side of (1.22) is dominated by the first term, which is *negative* for $b > 1$. The linear term thus pushes the step back into the bunch, and it can escape only thanks to the repulsive, nonlinear step-step interaction. Since the bunches become steeper with increasing size, the ability of a bunch to eject crossing steps also depends on the number of steps N that it contains.

The result of this interplay between linear and nonlinear effects is the phase diagram in the U - N -plane depicted in Fig.1.16. At moderate values of U it predicts a qualitative change in the behavior of bunches with increasing N . For small bunches the emission of steps ceases completely, such that all steps constituting the bunch move at the speed of the whole bunch and $V = 1$ in our units. Larger bunches emit one step at a time. Figure 1.17 shows the transition between the two regimes in a time-dependent situation. The initial condition consists of 4 small bunches of 16 steps each. These bunches initially merge in a

hierarchical fashion without exchanging steps. This behavior is characteristic of *strongly* conserved step dynamics [40,43], which in our units corresponds to $b \rightarrow \infty$. After the last merger the bunch enters the region in the phase diagram of Fig.1.16 where step emission is possible, and correspondingly the overall bunch motion slows down. It can also be seen that the emission of steps is accompanied by a periodic “breathing” of the entire bunch [46].

A rough estimate of experimental parameters indicates that both regimes $b < 1$ and $b > 1$ can be accessed in experiments on electromigration-induced step bunching of the Si(111) surface by varying the temperature [44]. The identification of the predicted phase transition is however not straightforward because real steps can bend [54], thus invalidating the one-dimensional approximation used throughout this section.

1.3.5

Coarsening

The time evolution depicted in Fig.1.17 is an example of *coarsening*, a term that is generally used to describe the (unlimited) increase of bunch size with time. In many cases coarsening proceeds according to a power law,

$$L \sim N \sim t^n \quad (1.25)$$

defining the coarsening exponent n . Despite recent progress in the theory of coarsening dynamics for one-dimensional fronts [55], a quantitative analysis of coarsening dynamics based on nonlinear continuum equations such as (1.17) seems still out of reach. Nevertheless, heuristic arguments (to be explained below) in combination with numerical [40,42] and experimental [56] evidence indicate that, as far as the weakly conserved system (1.14) including its strongly conserved limit is concerned, the coarsening exponent is

$$n = \frac{1}{2} \quad (1.26)$$

under a wide range of conditions; in particular, the value of n does not seem to be affected by the phase transition at $b = 1$ [57].

The first heuristic argument goes back to Chernov [58], and it is based on the relation (1.20) for the bunch velocity. The key assumption is that V is the only velocity scale in the problem, such that the velocity *difference* between two bunches of similar size $\sim N$ is also of order $\Delta V \sim 1/N$. The time required for two bunches to merge is then of order $L/\Delta V \sim N^2$, and (1.26) follows. A weakness of this argument is that it assumes coarsening to proceed by the merging of bunches, which does not need to be true when bunches can exchange steps.

The second argument, due to Liu and Weeks [42], is based on the generally conserved form of the continuum equation for the height profile $h(x, t)$, which

reads (in a frame where the constant rate of sublimation has been subtracted)

$$\frac{\partial h}{\partial t} + \frac{\partial j}{\partial x} = 0. \quad (1.27)$$

Without further specifying the current j , Liu and Weeks assume the existence of a single lateral length scale $\sim t^n$, such that both the height profile and the current take on scaling forms

$$h(x, t) = t^n H(x/t^n), \quad j(x, t) = J(x/t^n). \quad (1.28)$$

Inserting (1.28) into (1.27) enforces (1.26). Similar scaling arguments have been advanced by Pimpinelli and coworkers [50].

Like the argument of Chernov, the ansatz (1.28) is problematic because the bunch spacing is *not* the only length scale in the system [31, 45]; for example, the bunch width W defines a second (time-dependent) scale which cannot obviously be ignored. An explicit counterexample where the existence of an additional length scale leads to coarsening exponents which differ from (1.26) was presented in [49].

1.3.6

Nonconserved dynamics

In the presence of sublimation the rate of volume change (1.13) couples to the step configuration, and therefore the weakly conserved form of the discrete [Eq.(1.14)] and continuous [Eq.(1.17)] evolution equations is no longer appropriate [28]. The minimal modification of (1.14) which takes account of this fact reads [59]

$$\frac{dx_i}{dt} = (1 + gf_i) \left[\frac{1+b}{2}(x_i - x_{i-1}) + \frac{1-b}{2}(x_{i+1} - x_i) \right] + U(2f_i - f_{i+1} - f_{i-1}), \quad (1.29)$$

where the new dimensionless parameter g is proportional to the strength of the repulsive step-step interactions. On the linearized level the introduction of the new term shifts the instability condition, which now reads [48, 59]

$$b > 6g. \quad (1.30)$$

The nonlinear consequences of the new term are quite dramatic. Numerical simulations of (1.29) [60], as well as of a more complicated non-conserved model [40] show that the coarsening of step bunches is *arrested* when the bunches have reached a certain size. Correspondingly, a large initial step bunch evolving under the dynamics (1.29) breaks up into smaller bunches, as illustrated in Fig.1.18.

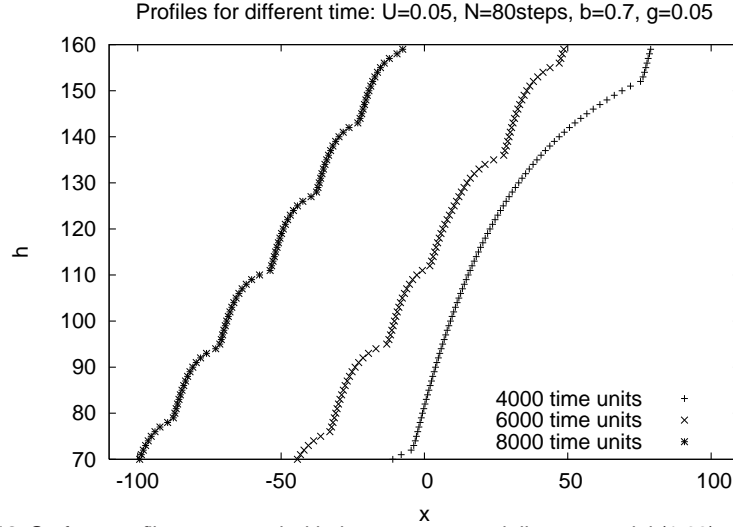


Fig. 1.18 Surface profiles generated with the nonconserved discrete model (1.29) with parameters $b = 0.7$ and $U = g = 0.05$. The initial condition is a single large bunch, which first relaxes into a quasi-stationary configuration and then breaks up into smaller bunches after 4000 time steps. Height profiles at different times have been shifted in the horizontal direction.

The absence of (asymptotic) coarsening in the nonconserved case is consistent with analyses in which *weakly* nonlinear continuum equations (in the sense of [61]) are derived from the discrete step dynamics close to the instability threshold, i.e. for $1 - 6g/b \ll 1$ [62,63]. These equations typically display spatio-temporal chaos or structure formation at a fixed length scale, but no coarsening [31]. However, for strongly nonlinear continuum equations similar to (1.17), which are expected to apply when $b \gg g$, such results are so far not available.

1.3.7

Beyond the quasistatic approximation

With few exceptions [64–66], most theoretical studies of step dynamics work in the *quasistatic* approximation, which implies that the dynamics of the diffusing adatoms on the terraces separating the steps is assumed to be much faster than the step motion. As a consequence a step reacts instantaneously to the motion of its neighbors, which mathematically leads to coupled first-order equations for the step positions such as (1.14).

A simple and conceptually appealing way of explicitly including the time scale of adatom dynamics was recently proposed by Ranguelov and Stoyanov, who derived and studied a coupled system of two sets of evolution equations, one for the terrace widths $l_i = x_{i+1} - x_i$ and one for the (suit-

ably parametrized) adatom concentration profile on the terraces. Remarkably, in this setting the equidistant step train may undergo an instability into a new dynamic phase characterized by step compression waves [67], even if it would be completely stable in the quasistatic limit. The instability is caused solely by the time delay that is introduced into the interaction between steps by the finite time scale of the adatom dynamics, similar to the instabilities induced in follow-the-leader models of highway traffic by the finite reaction time of drivers [52, 53]. In the presence of electromigration and sublimation, the non-quasistatic model reproduces the main features of the phase transition described above in Sect.1.3.4 [68].

1.4

Conclusions

The fact that the evolution of nanostructures is intrinsically noisy is by now widely appreciated [1]. In contrast, the role of deterministic nonlinear dynamics, in the sense of dynamical systems theory, as a source of complex behavior is largely unexplored in this context. Here I have presented the results of two case studies in which concepts from nonlinear dynamics appear naturally in the analysis of the evolution of surface nanostructures. In both cases surface steps constitute the relevant degrees of freedom which, despite satisfying simple equations of motion, can display a wide range of dynamic phenomena. Many other systems, not discussed here, fit into the same framework; an example of current interest is the thermal decay of nanoscale mounds, either through the periodic collapse of the top island [69] or through the jerky rotation of a spiral step emanating from a screw dislocation [70]. It should have become clear that much, perhaps most of the work in this field remains to be done.

Acknowledgements

This chapter is based on joint work with Frank Hausser, Marian Ivanov, Philipp Kuhn, Vladislav Popkov, Marko Rusanen, and Axel Voigt. I am grateful to Dionisios Margetis, Olivier Pierre-Louis, Alberto Pimpinelli, Paolo Politi, Bogdan Rangelov, Stoyan Stoyanov, Vesselin Tonchev and John D. Weeks for useful interactions, and to DFG for support within SFB 616 *Energy dissipation at surfaces* and project KR 1123/1-2.

Bibliography

- 1 Williams, E.D., *MRS Bulletin* September (2004), p.621
- 2 Burton, W. K., Cabrera, N., Frank, F. C., *Phil. Trans. Roy. Soc. A* 243 (1951), p.299
- 3 Jeong, H.-C., Williams, E. D., *Surf. Sci. Rep.* 34 (1999), p.171
- 4 Giesen, M., *Prog. Surf. Sci.* 68 (2001), p.1
- 5 Michely, T., Krug, J., *Islands, Mounds and Atoms. Patterns and Processes in Crystal Growth Far from Equilibrium*, Springer, Berlin, 2004
- 6 Pierre-Louis, O., *C. R. Physique* 6 (2005), p.11
- 7 Evans, J. W., Thiel, P. A., Bartelt, M. C., *Surf. Sci. Rep.* 61 (2006), p.1
- 8 Krug, J., in *Multiscale Modeling in Epitaxial Growth*, (Ed.: A. Voigt) Birkhäuser, Basel 2005, p.69
- 9 Tu, K. N., *J. Appl. Phys.* 94 ((2003), p.5451
- 10 Bondarchuk, O., Cullen, W. G., Degawa, M., Williams, E. D., Bole, T., Rous, P. J., *Phys. Rev. Lett.* 99 (2007), 206801
- 11 Métois, J.-J., Heyraud, J.-C., Pimpinelli, A., *Surf. Sci.* 420 (1999), p.250
- 12 Pierre-Louis, O., Einstein, T. L., *Phys. Rev. B* 62 (2000), p.13697
- 13 Ho, P. S., *J. Appl. Phys.* 41 (1970), p.64
- 14 Wang, W., Suo, Z., Hao, T.-H., *J. Appl. Phys.* 79 (1996), p.2394
- 15 Kuhn, P., Krug, J., in *Multiscale Modeling in Epitaxial Growth*, (Ed.: A. Voigt) Birkhäuser, Basel 2005, p.159
- 16 Kuhn, P., *Nichtlineare Dynamik von Oberflächeninseln unter Elektromigrationseinfluss*, PhD Dissertation, Universität zu Köln, 2007
- 17 Kuhn, P., Krug, J., Hausser, F., Voigt, A., *Phys. Rev. Lett.* 94 (2005), 166105
- 18 Schimschak, M., Krug, J., *J. Appl. Phys.* 87 (2000), p.695
- 19 Rusanen, M., Kuhn, P., Krug, J., *Phys. Rev. B* 74 (2006), 245423
- 20 Mehl, H., Biham, O., Millo, O., Karimi, M., *Phys. Rev. B* 61 (2000), p.4975
- 21 Gungor, M. R., Maroudas, D., *Surf. Sci.* 461 (2000), p.L550
- 22 Cho, J., Gungor, M. R., Maroudas, D., *Surf. Sci.* 602 (2008), p.1227
- 23 Cho, J., Gungor, M. R., Maroudas, D., *Appl. Phys. Lett.* 86 (2005), 241905
- 24 Hausser, F., Kuhn, P., Krug, J., Voigt, A., *Phys. Rev. E* 75 (2007), 046210
- 25 Schimschak, M., Krug, J., *Phys. Rev. Lett.* 80 (1998), p.1674
- 26 Meulenbroek, B., Ebert, U., Schäfer, L., *Phys. Rev. Lett.* 95 (2005), 195004
- 27 Ebert, U., Meulenbroek, B., Schäfer, L., *SIAM J. Appl. Math.* 68 (2007), p.292
- 28 Pierre-Louis, O., *Surf. Sci.* 529 (2003), p.114
- 29 Néel, N., Maroutian, T., Douillard, L., Ernst, H.-J., *Phys. Rev. Lett.* 91 (2003), 226103
- 30 Yu, Y.-M., Liu, B.-G., *Phys. Rev. B* 73 (2006), 035416
- 31 Krug, J., in *Collective Dynamics of Nonlinear and Disordered Systems*, (Eds.: G. Radons, W. Just, P. Häussler) Springer, Berlin, 2005, p.5
- 32 Schwoebel, R.L., Shipsey, E.J., *J. Appl. Phys.* 37 (1966), p.3682
- 33 Schwoebel, R.L., *J. Appl. Phys.* 40 (1969), p.614
- 34 Stoyanov, S., *Jap. J. Appl. Phys.* 30 (1991), p.1
- 35 Kandel, D., Weeks, J.D., *Phys. Rev. Lett.* 69 (1992), p.3758
- 36 Kandel, D., Weeks, J.D., *Physica D* 66 (1993), p.78
- 37 van der Eerden, J.P., Müller-Krumbhaar, H., *Physica Scripta* 40 (1989), p.337
- 38 Vollmer, J., Hegedüs, J., Grosse, F., Krug, J., *New J. Phys.* 10 (2008), 053017
- 39 Krug, J., *Adv. Compl. Systems* 4 (2001), p.353
- 40 Sato, M., Uwaha, M., *Surf. Sci.* 442 (1999), p.318
- 41 Krug, J., *Adv. Phys.* 46 (1997), p.139
- 42 Liu, D.-J., Weeks, J.D., *Phys. Rev. B* 57 (1998), p.14891
- 43 Chang, J., Pierre-Louis, O., Misbah, C., *Phys. Rev. Lett.* 96 2006, 195901
- 44 Popkov, V., Krug, J., *Europhys. Lett.* 72 (2005), p.1025
- 45 Krug, J., Tonchev, V., Stoyanov, S., Pimpinelli, A., *Phys. Rev. B* 71 (2005), 045412

- 46 Popkov, V., Krug, J., *Phys. Rev. B* 73 (2006), 235430
- 47 Krug, J., in *Dynamics of Fluctuating Interfaces and Related Phenomena*, (Ed.: D. Kim, H. Park and B. Kahng) World Scientific, Singapore 1997, p.95
- 48 Fok, P.-W., Rosales, R. R., Margetis, D., *Phys. Rev. B* 76 (2007), 033408
- 49 Slanina, F., Krug, J., Kotrla, M., *Phys. Rev. E* 71 (2005), 041605
- 50 Pimpinelli, A., Tonchev, V., Videcoq, A., Vladimirova, M. *Phys. Rev. Lett.* 88 (2002), 206103
- 51 Fujita, K., Ichikawa, M., Stoyanov, S., *Phys. Rev. B* 60 (1999), p.16006
- 52 Chowdhury, D., Santen, L., Schadschneider, A., *Phys. Rep.* 329 (2000), p.199
- 53 Helbing, D., *Rev. Mod. Phys.* 73 (2001), p.1067
- 54 Thürmer, K., Liu, D.-J., Williams, E.D., Weeks, J.D., *Phys. Rev. Lett.* 83 (1999), p.5531
- 55 Politi, P., Misbah, C., *Phys. Rev. E* 73 (2006), 036133
- 56 Yang, Y.-N., Fu, E.S., Williams, E.D., *Surf. Sci.* 356 (1996), p.101
- 57 Ranguelov, B., Tonchev, V. (unpublished)
- 58 Chernov, A., *Sov. Phys. Usp.* 4 (1961), p.116
- 59 Ivanov, M., *Dynamik von Stufen auf vizinalen Kristalloberflächen*, Diploma thesis, Universität zu Köln, 2007
- 60 Ivanov, M., Popkov, V., Krug, J. (unpublished)
- 61 Pierre-Louis, O., *Europhys. Lett.* 72 (2005), p.894
- 62 Sato, M., Uwaha, M., *Europhys. Lett.* 32 (1995), p.639
- 63 Misbah, C., Pierre-Louis, O., *Phys. Rev. E* 53 (1996), p.R4318
- 64 Ghez, R., Iyer, S.S., *IBM J. Res. Dev.* 32 (1988), p.804
- 65 Ghez, R., Cohen, H.G., Keller, J.B., *J. Appl. Phys.* 73 (1993), p.3685
- 66 Keller, J.B., Cohen, H.G., Merchant, G.J., *J. Appl. Phys.* 73 (1993), p.3694
- 67 Ranguelov, B., Stoyanov, S., *Phys. Rev. B* 76 (2007), 035443
- 68 Ranguelov, B., Stoyanov, S., *Phys. Rev. B* 77 (2008), 205406
- 69 Margetis, D., Fok, P.-W., Aziz, M.J., Stone, H.A., *Phys. Rev. Lett.* 97 (2006), 096102
- 70 Ranganathan, M., Dougherty, D.B., Cullen, W.G., Zhao, T., Weeks, J.D., Williams, E.D., *Phys. Rev. Lett.* 95 (2005), 225505